J. of Supercritical Fluids 53 (2010) 142–150

Contents lists available at ScienceDirect

The Journal of Supercritical Fluids

journal homepage: www.elsevier.com/locate/supflu

Electrospinning in compressed carbon dioxide: Hollow or open-cell fiber formation with a single nozzle configuration

Jun Liu[a], Zhihao Shen[b], Sang-Ho Lee[c], Manuel Marquez[d], Mark A. McHugh[a,*]

[a] Department of Chemical and Life Science Engineering, Virginia Commonwealth University, VCU, 601 West Main St., Richmond, VA 23284, USA
[b] Beijing National Laboratory for Molecular Sciences, Key Laboratory of Polymer Chemistry and Physics of Ministry of Education, College of Chemistry and Molecular Engineering, Peking University, Beijing 100871, China
[c] Department of Chemical Engineering, Dong-A University, Busan, South Korea
[d] YNano LLC, 14148 Riverdowns South Dr., Midlothian, VA 23113, USA

ARTICLE INFO

Article history:
Received 14 August 2009
Received in revised form 12 February 2010
Accepted 13 February 2010

Keywords:
Open-cell and hollow fibers
Electrospinning
Compressed carbon dioxide

ABSTRACT

Electrospinning is combined with the PCA (precipitation with a compressed fluid antisolvent) process (ES–PCA) to produce micron to submicron polymeric fibers with open-cell or hollow core morphology. CO_2 is used as the compressed gas of choice and the impact of CO_2 pressure (density) on fiber morphology is demonstrated for the poly(vinyl pyrrolidone) (PVP)–dichloromethane, PVP–ethanol, poly(vinylidenefluoride) (PVDF)–dimethylacetamide, and PVDF–dimethyl formamide systems. CO_2, which is in excess for this process, rapidly extracts solvent from the surface of the liquid jet to form a vitrified polymer skin and also dissolves into the liquid jet and induces the polymer–solvent solution to phase separate. The ES–PCA technique has the advantage that fiber morphology can be easily controlled via pressure and pressures in excess of 100 bar are not needed to obtain a variety of different fiber morphologies. The fiber formation process correlates closely with the binary solvent–CO_2 and ternary polymer–solvent–CO_2 phase behavior.

1. Introduction

It is now well known that polymer fibers exhibit several unique characteristics as the fiber diameter shrinks from micrometer to submicron-to-nanometer dimensions. These fibers have a very large surface area to volume ratio which magnifies the impact of any surface functionality and often improves the mechanical performance characteristics of the fiber [1,2] thus expanding the range of applications of nanofibrous scaffolds [1,3]. Electrospinning is emerging as one of the most intriguing methods for the production of polymeric nanofibers [1–4]. The electrospinning process has characteristics similar to other commercial processes for drawing microscale fibers although electrospinning uses the electrostatic repulsions between surface charges to continuously reduce the diameter of a viscoelastic jet to produce micron- or nano-size fiber [5]. In 1995 Doshi and Reneker [6] showed electrospinning to be a viable fiber spinning technique for producing submicron diameter fibers. In fact, in the last decade, there has been an exponential increase in the number of electrospinning publications reporting how fiber properties are controlled by the magnitude of the electric field, the polymer–solvent solution properties such as viscosity and solvent volatility, and the apparatus configuration such as the distance between the nozzle and target, the configuration of the target, and the spinning bath environment [2,5,7,8].

For certain applications it is desirable to control the diameter, internal morphology, and the surface structure of a fiber. For example, porous fibers or fibers with a large surface-to-volume ratio are preferred for filter applications or as templates for forming functional nanotubes [9]. The electrospinning process can be used to create fibers with surface porosity if a highly volatile solvent is used [10,11]. The removal of solvent from the surface of the liquid jet can result in a porous fiber skin as residual solvent evaporates from the nascent fiber. The humidity of the electrospinning environment can also induce surface structure as water evaporates from the fiber surface [11,12]. If the fiber collector is immersed in a cryogenic liquid, highly porous fibers are produced by the very fast temperature-induced, polymer–solvent phase separation followed by removal of the solvent upon subsequent heating of the fiber [13]. Porous polymer fibers can also be generated by electrospinning polymer blends followed by the selective removal of one of the polymers [14]. Alternatively, several research groups have created hollow or porous fibers by electrospinning with a coaxial spinneret capable of delivering two immiscible solutions that results in a liquid jet within a jet. The fiber produced in this process has a core–shell morphology in which the core material is subsequently removed

* Corresponding author. Tel.: +1 804 827 7031.
E-mail address: mmchugh@vcu.edu (M.A. McHugh).

0896-8446/$ – see front matter © 2010 Elsevier B.V. All rights reserved.
doi:10.1016/j.supflu.2010.02.016

by a post-fiber-spinning solvent extraction or thermal treatment step [15–19].

A versatile method for forming microporous polymer fibers or asymmetric porous membranes is to induce a phase separation with a nonsolvent [20,21]. In this instance pores are created when the solvent-rich phase is removed from the vitrified polymer. In the wet-spinning process the solution jet is spun into a bath containing liquid nonsolvent where a nonsolvent–solvent exchange occurs causing the solution in the jet to phase separate [21]. In an alternative processing scheme the solution jet is directed into a spinning bath containing nonsolvent vapor that rapidly diffuses into the solution jet and induces a phase separation [21]. The application of a nonsolvent vapor suggests the potential of using a high-pressure gas, or a supercritical fluid solvent as the nonsolvent in an electrospinning process [22].

Compressed CO_2 is an intriguing candidate nonsolvent gas given its interesting physical properties and potential as a processing aid [23]. CO_2, at low to moderate pressures, is a very poor solvent for virtually all polymers [24], including poly(vinyl pyrrolidone) (PVP) [25], while at the same operating conditions CO_2 can solubilize most organic solvents including acids, alcohols, and other low volatility solvents. In a process called "precipitation with a compressed fluid antisolvent" (PCA), several groups have created short, hollow or porous, micro-fibers by spraying a polymer–solvent solution through a capillary tube into a CO_2 bath at conditions where CO_2 rapidly extracts the solvent from the polymer–solvent jet [26,27]. Near-critical or supercritical CO_2 more rapidly diffuses into the polymer–solvent liquid jet and more rapidly extracts the solvent compared to the mass transfer and extraction rates experienced when spinning into a liquid antisolvent bath [23,28].

The influx of CO_2 into the liquid jet rapidly induces the solution to phase separate into polymer-rich and solvent-rich phases. CO_2 reduces the strength of the organic solvent for two reasons. As mentioned, CO_2 is a poor solvent for most polymers and, therefore, adding CO_2 to a high-quality polymer solvent creates a mixed solvent of inferior quality. CO_2 also dilates the polymer solvent, which increases the difference in free volume or, equivalently, thermal expansivity, between the polymer and the solvent that can result in a phase separation, a process first reported in 1960 and further developed in the early 1970s [29,30]. The free-volume difference can be created by heating the polymer solution to temperatures near the critical temperature of the organic solvent. However, in the early 1980s several research groups demonstrated that phase separation, via a free-volume difference mechanism, can occur, isothermally, with the addition of a low molecular weight supercritical fluid solvent to the polymer solution [31,32]. It is important to note that a nascent dry fiber is quickly formed when the jet enters the CO_2 bath due to the rapid extraction of solvent from the surface of the jet that creates a vitrified polymer skin. The solvent power of a compressed gas or a supercritical fluid can be adjusted by pressure as well as temperature, which means that the operating pressure can be used to control the rate of solvent extraction from the liquid polymer–solvent jet and the amount of gas dissolved in the jet [26]. Another advantage with this CO_2-induced phase separation and solvent extraction process is the potential to operate at moderate-to-low temperatures thus making it viable to process thermally labile polymers or polymer solutions containing thermally labile additives, such as drugs.

In a previous study, we reported on a combined electrospinning–PCA (ES–PCA) technique to create porous polymer fibers [22]. The present work describes an improved experimental apparatus capable of electrospinning with near critical and supercritical fluids. CO_2 is used as the compressed gas of choice, although other gases could be used, such as ethane. The impact of CO_2 pressure (density) on the resultant fiber morphology is demonstrated for the PVP–dichloromethane (DCM), PVP–ethanol, poly(vinylidenefluoride) (PVDF)–dimethylacetamide (DMAc), and PVDF–dimethyl formamide (DMF) systems.

PVP–DCM electrospinning is performed at room temperature (~22 °C) and at 35 °C, which are temperatures very close to the normal boiling point of DCM (T_{boil} = 40 °C). Data are presented to show how the internal fiber microstructure can be controlled by spinning into a CO_2 bath at different operating pressures. Literature DCM–CO_2 phase behavior data [33,34] are used to provide insight into the ability of CO_2 to extract DCM from the liquid jet, which leads to the formation of a polymer skin on the liquid jet. To match the binary data to specific electrospinning temperatures and pressures, the Peng–Robinson equation of state is used with conventional mixing rules [35] and an interaction parameter, k_{ij}, equal to 0.050, which provides a good fit of the available literature data. As a complement to the binary DCM–CO_2 data, phase behavior data are obtained in the present study for a 5.2 wt% PVP–81.3 wt% DCM–13.5 wt% CO_2 and a 4.8 wt% PVP–63.4 wt% DCM–31.8 wt% CO_2 ternary mixture that both contain ~6.0 wt% PVP in DCM on a CO_2-free basis, similar to the PVP levels in the spinning solution. The phase behavior data for the ternary mixture with 13.5 wt% CO_2 provides information on the conditions needed to extract DCM from the surface of the polymer solution jet, while the data for the ternary mixture with 31.8 wt% CO_2 ternary mixture provides an indication of how strongly CO_2 promotes the phase separation of the DCM–PVP solution in the interior of the jet.

PVP–ethanol electrospinning experiments are performed at room temperature where ethanol is ~8 times less volatile than DCM. Although solid-core PVP fibers can be obtained by electrospinning PVP–ethanol solutions into air, it is shown that PVP fibers with an internal, open-cell structure can be obtained when electrospinning into a CO_2 bath. In contrast, PVDF is problematic to electrospin into air since the typical solvents for this polymer, such as DMAc and DMF, exhibit very low volatility at near ambient temperatures. Other researchers have successfully electrospun PVDF and other difficult-to-dissolve polymers if a volatile liquid cosolvent, such as acetone, is used to increase the vapor pressure of the primary solvent [36–40]. In the present study results are presented showing that PVDF fibers with internal, open-cell structure can be created by electrospinning PVDF–DMAc and PVDF–DMF solutions into a CO_2 bath at room temperature. The different PVDF fiber morphologies are a manifestation of the versatility of using CO_2 as a processing aid for fiber spinning with low volatility solvents given that DMAc and DMF are more than 100 times less volatile than DCM at room temperature. It is also noted that the impact of the binary phase behavior for the ethanol–CO_2, DMAc–CO_2 [41], and DMF–CO_2 [42] systems is expected to be similar to that of the DCM–CO_2 system since the pressure–composition isotherms for all four binary mixtures exhibit identical trends and have similar values of pressure. Hence, only the DCM–CO_2 phase behavior is described in detail.

1.1. Experimental

In our previous study an all-metal apparatus was used for electrospinning into a CO_2 bath at pressures near 100 bar [22]. A significant limitation of this original apparatus was that only short fibers were produced due to the very short nozzle-to-target distance of ~2.5 cm. If the nozzle-to-target distance was increased beyond ~2.5 cm, the polymer jet traveled to the inside surface of the high-pressure vessel rather than to the target even when operating at potentials greater than 15 kV. The main features of the redesigned electrospinning apparatus, shown in Fig. 1, consist of a pressure vessel, a high-voltage power supply, a high-pressure syringe pump for injecting polymer solution, and a high-pressure compressor for injecting CO_2. The nozzle-to-target distance is ~8.5 cm, which is more than three times longer than the distance

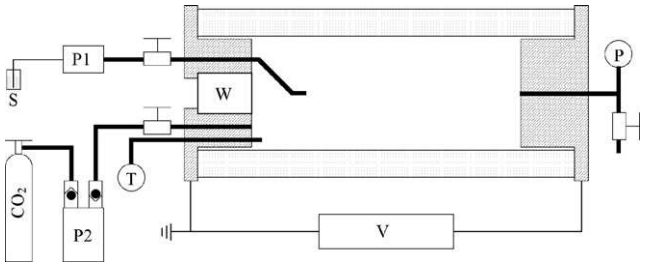

Fig. 1. Schematic diagram of the high-pressure, electrospinning apparatus used in this study. P, pressure gauge; P1 and P2, solvent and CO_2 pumps, respectively; S, polymer solution storage; T, temperature sensor; W, sapphire window; V, voltage supply.

in the original apparatus [22] and is just slightly shorter than the typical nozzle-to-collector distances reported in the literature. The original and redesigned apparatus both use o-rings to make pressure seals which means that the maximum operating temperature in each case is limited by the temperature rating of the o-rings, which typically do not exceed 150 °C unless teflon o-rings are used.

A nonconductive PEEK tube (6.35 cm ID, 7.62 cm OD, ~400 ml volume), used to house the nozzle and target, is sealed by o-rings onto two, stainless steel end plates mounted on a nonconductive plastic base. The end plate with the nozzle is fitted with a sapphire window, sealed by an o-ring, to allow for observation of the inside of the vessel using a borescope (Olympus Corporation, model F100-024-000-55) connected to a video monitor. A high-pressure compressor (Superpressure Inc., model 46-14025-1) is used to inject CO_2 into the vessel and an isocratic pump (ChromTech, model ISO-100) or a syringe pump (Harvard Apparatus, model PHD 4400) is used to deliver polymer solution to the 316 stainless steel, grounded nozzle (0.159 cm OD and 0.076 cm ID). A platinum resistance thermal device (RTD) is inserted into the vessel to measure the temperature and the system pressure is measured with a digital pressure transducer (GE Sensing, Druck DPI 104). A high-voltage power supply (Spellman, model CZE1000R) is used to apply 0–30 kV to the right-side end cap. The new apparatus is easy to disassemble for recovering fiber and it can operate to pressures as high as 135 bar while maintaining a safety factor of four based on accepted pressure vessel standards [43].

The vessel is heated to the desired operating temperature and then charged with CO_2 to the desired pressure. A premixed polymer solution is pumped through the nozzle at a flow rate of ~0.20 ml/min. Once the polymer solution starts to drip from the nozzle tip, the flow rate is reduced to ~0.01 ml/min and a 15–30 kV voltage is applied to start the electrospinning process that typically lasts for 15 min at each set of operating conditions to obtain a very small, but sufficient, amount of fiber for SEM analysis. The focus here is to determine the impact of operating conditions on the fiber morphology rather than to optimize the fiber production rate. Fiber samples recovered from the high-pressure vessel are cooled in liquid nitrogen and cut with a razor blade to reveal the internal fiber morphology. The fibers are placed on carbon tape and sputter coated for SEM (JEOL JSM-820 and Zeiss EVO 50XVP) analysis.

Described elsewhere are the techniques used to obtain cloud-point curves for the PVP–DCM–CO_2 ternary mixtures [44]. Cloud points are measured and reproduced at least twice to within ±1.4 bar and ±0.5 °C. The cloud-point pressure is defined as the point at which the solution becomes so opaque that it is no longer possible to see the stir bar in solution.

1.2. Materials

PVP (Aldrich, weight average molecular weight = 1,300,000 g mol^{-1}) and PVDF (weight average molecular weight = 275,000 g mol^{-1}, number average molecular weight = 107,000 g mol^{-1}) were purchased from Sigma–Aldrich and used as received. It is important to note that the formation of fiber, rather than polymer droplets, is related to the extent of polymer chain entanglement in solution, a condition characterized as polymer chain overlap. The higher the polymer molecular weight, the lower the polymer concentration needed to obtain chain overlap in solution and the lower the polymer concentration needed to obtain fibers. In an extensive electrospinning study, McKee and coworkers elucidate the dependence of molecular weight on fiber formation and show that even polymers with modest molecular weight, such as the PVDF used in the present study, can be used to create fibers spun from solutions with low to moderate polymer concentrations [45]. The next section of the present manuscript presents CO_2-assisted electrospinning results on the impact of polymer concentration on fiber morphology for a high molecular weight PVP and a more modest molecular weight PVDF.

The DCM (99.5+%) was purchased from Alfa Aesar and used as received. The DMAc (99% minimum), ethanol (absolute, ≥99.5%), and DMF (99.5% minimum) were purchased from Sigma–Aldrich and used as received. Medical grade CO_2 was purchased from Roberts Oxygen and used as received.

2. Results and discussion

2.1. Electrospinning PVP–DCM

Fig. 2 shows the PVP fibers produced by electrospinning a 6.5 wt% PVP–DCM solution into CO_2 at 34 °C. Fiber diameters of ~1 μm are produced at a CO_2 pressure of 8 bar (Fig. 2(A)) although many fibers are fused together suggesting that the polymer skin of the fibers was not vitrified by the time the fiber reached the target. At 8 bar and 34 °C the calculated solubility of CO_2 in the DCM-rich phase is only ~5 wt% and the calculated solubility of DCM in the CO_2-rich phase is ~20 wt%. More importantly, the CO_2-rich, gas phase only has a calculated density of ~0.015 g/ml which suggests that CO_2 does not have sufficient solvent strength to extract much DCM from the surface of the solution jet. Hence, the low operating pressure and short time-of-flight of the solution jet from the nozzle to the target ensures that the CO_2 near the surface of the jet likely becomes quickly saturated with low amounts of DCM and the jet remains liquid-like when it hits the target. Fig. 2(D) shows that the PVP–DCM–CO_2 ternary mixture is also in a two-phase, liquid–vapor region of the phase diagram at 34 °C and 8 bar, corroborating that CO_2 indeed has low solvent strength at this very low pressure.

When the CO_2 pressure is increased to 22 bar (Fig. 2(B)) the resultant fiber has a solid core and a diameter similar to that observed at 8 bar, although these fibers are not fused together. At 22 bar and 34 °C the calculated solubility of CO_2 in the DCM-rich phase is now ~16 wt% and the solubility of DCM in the CO_2-rich phase drops to ~8 wt%, however, the density of the CO_2-rich gas phase is ~0.045 g/ml, which is three times more dense than that observed at 8 bar. Hence, the solvent power of CO_2 has increased considerably even at these very low pressures. Fig. 2(D) shows that the bubble-point, liquid + vapor ⇒ liquid phase transition at 34 °C for the PVP–DCM–CO_2 ternary mixture occurs at ~20 bar. The conditions needed for the formation of dry, solid-core PVP fiber correlates well with the ternary phase behavior. It is difficult, however, to postulate a one-to-one correspondence between fiber spinning, which is a dynamic process, and phase behavior measurement, which is a static experiment. At the start of an electrospinning experiment at 22 bar and 34 °C there are ~17 g of CO_2 in the PEEK vessel and the 6.5 wt% PVP–DCM solution flows into the vessel at ~0.01 ml/min, which translates to ~0.013 g DCM/min. Even after

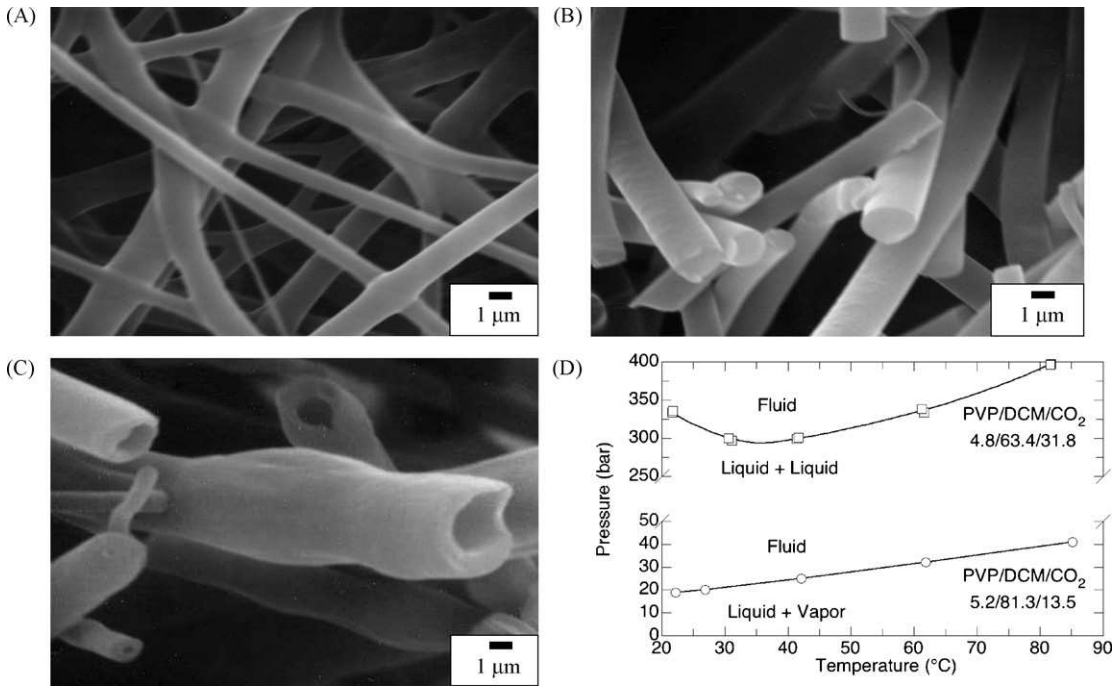

Fig. 2. SEM micrographs of PVP fibers created by electrospinning a 6.5 wt% PVP–DCM solution into pure CO_2 at 34 °C and 8 bar (A), 22 bar (B), and 35 bar (C). (D) Impact of CO_2 on the location of the PVP–DCM phase boundary obtained in this study; note the break in the pressure axis.

15 min, the CO_2-rich phase is far from being saturated in DCM. CO_2, which is in excess, not only extracts DCM from the liquid jet, but also dissolves into the liquid jet and induces the PVP–DCM solution to phase separate. Given that the fiber diameter is ~1.5 μm (see Fig. 2(B)), a significant amount of CO_2 rapidly diffuses 0.50–0.75 μm into the liquid jet within ~0.3 ms assuming a diffusion coefficient of 1.0×10^{-6} cm^2/s for CO_2 in the solution jet.[22] It is also worth noting that the 4.8 wt% PVP–63.4 wt% DCM–31.8 wt% CO_2 cloud-point curve shown in Fig. 2(D) is located at ~275 bar at 34 °C, which implies that a CO_2-rich bubble phase and a PVP-rich liquid phase are rapidly formed in the central portion of the jet at the low pressure of 22 bar. Many of the trends observed for the PVP–DCM–CO_2 system are similar to those reported by Bae et al. [25] for the PVP–vinyl pyrrolidone (VP)–CO_2 system although in this latter case the highest weight-average molecular weight of PVP was only 40,000, the operating temperatures were 50 °C and higher, and the highest amount of VP cosolvent investigated was only 36.6 wt%. The high CO_2 solvent power for DCM, the low solvent power of CO_2 for PVP, and the short time needed for CO_2 to diffuse 0.50–0.75 μm into the liquid jet, are conditions that favor the rapid formation of a vitrified PVP skin encasing a polymer–solvent solution undergoing spinodal decomposition.

At a CO_2 operating pressure of 35 bar, dry, hollow core fibers are obtained as shown in Fig. 2(C). The hollow core diameters are typically 1–2 μm, the skin thickness is ~0.50–0.75 μm, and the fiber diameters are slightly larger than those spun at lower pressures. Some fibers have bulges likely due to the rapid removal of DCM from the nascent, malleable jet. At 35 bar and 34 °C the calculated solubility of CO_2 in the DCM-rich phase is now ~29 wt% and the calculated solubility of DCM in the CO_2-rich gas phase is ~6 wt%. The density of the CO_2-rich gas phase is now ~0.080 g/ml, almost twice as dense as that at 22 bar. Given the large excess of CO_2 in the receiver vessel and the pressure of the two-phase boundary curve in Fig. 2(D) at 34 °C, it is reasonable to assume that the CO_2 concentration in the liquid PVP–DCM jet quickly exceeds 25 wt%. CO_2 induces the PVP–DCM solution to undergo spinodal decomposition resulting in a network of PVP–DCM solution interspersed with CO_2-rich bubbles. As the jet travels to the target the CO_2-rich bubbles continue to coalesce and expand against the PVP-rich network and the bubbles push the polymer-rich phase radially outward against the inner surface of the jet, thus creating a hollow core. However, there is a small operating pressure window for creating fibers with this electrospinning process. If the operating pressure is increased to 55 bar, CO_2 extracts DCM so rapidly from the liquid jet, that the nozzle will clog.

Fig. 3 shows the fibers created by operating at room temperature with sub-critical CO_2. It is possible to electrospin the 6.5 wt% PVP–DCM solution at ambient conditions and create fibers with 2–30 μm diameters. However, electrospinning at these conditions is problematic due to the high solution viscosity. In contrast, 0.25–1.0 μm diameter fibers are readily produced by electrospinning at 16 bar (Fig. 3(B)) using the apparatus shown in Fig. 1. Some of these fibers also contain ~8 μm diameter beads that generally result from electrospinning at polymer concentrations lower than the chain entanglement concentration [46]. At 16 bar the influx of CO_2 into the solution jet lowers the solution viscosity and makes fiber spinning more facile, but it also allows for the production of beads. When the CO_2 pressure is increased to 22 bar, the fiber diameter decreases to ~400 nm, Fig. 3(C), but again many fibers have beads that are slightly larger than those created at 16 bar. Although even smaller diameter fibers are created at 30 bar CO_2, most of the fibers contain beads and spindles as shown in Fig. 3(D). All the fibers shown in Fig. 3 have solid cores.

Porous, bead-free fibers are produced when the 6.5 wt% PVP–DCM solution is electrospun into sub-critical CO_2 at room temperature (~22 °C) and 35–50 bar. Fig. 4(A) shows hollow core fibers with diameters of ~2 μm produced at a CO_2 operating pressure of 35 bar, similar to those fibers produced at 34 °C and the same pressure. These fibers do not have beads, but a few of them do have bulges. When the CO_2 pressure is increased to 42 bar, the fibers, shown in Fig. 4(B), have larger, more uniform diameters compared with those spun at 35 bar CO_2. In addition, the fibers formed at 42 bar CO_2 have an internal open-cell structure. When spun at a CO_2 operating pressure of 50 bar, the fibers have much larger diameters and the distribution of fiber diameters increases likely due to the rapid vitrification of the jet skin which precludes the possibility of

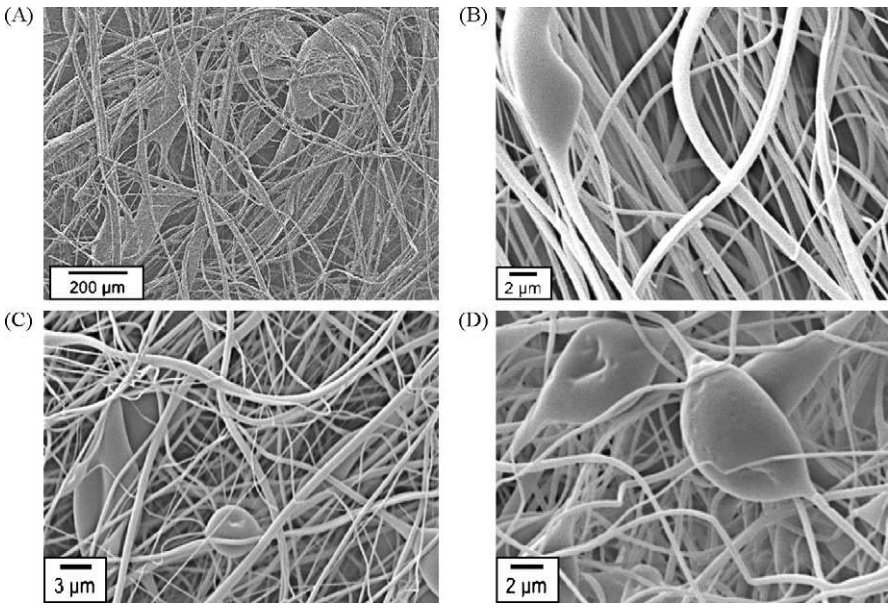

Fig. 3. SEM micrographs of PVP fibers created by electrospinning a 6.5 wt% PVP–DCM solution at room temperature (~22 °C) and ambient pressure (A) and spinning at 22 °C and into CO_2 at 16 bar (B), 22 bar (C), and 30 bar (D).

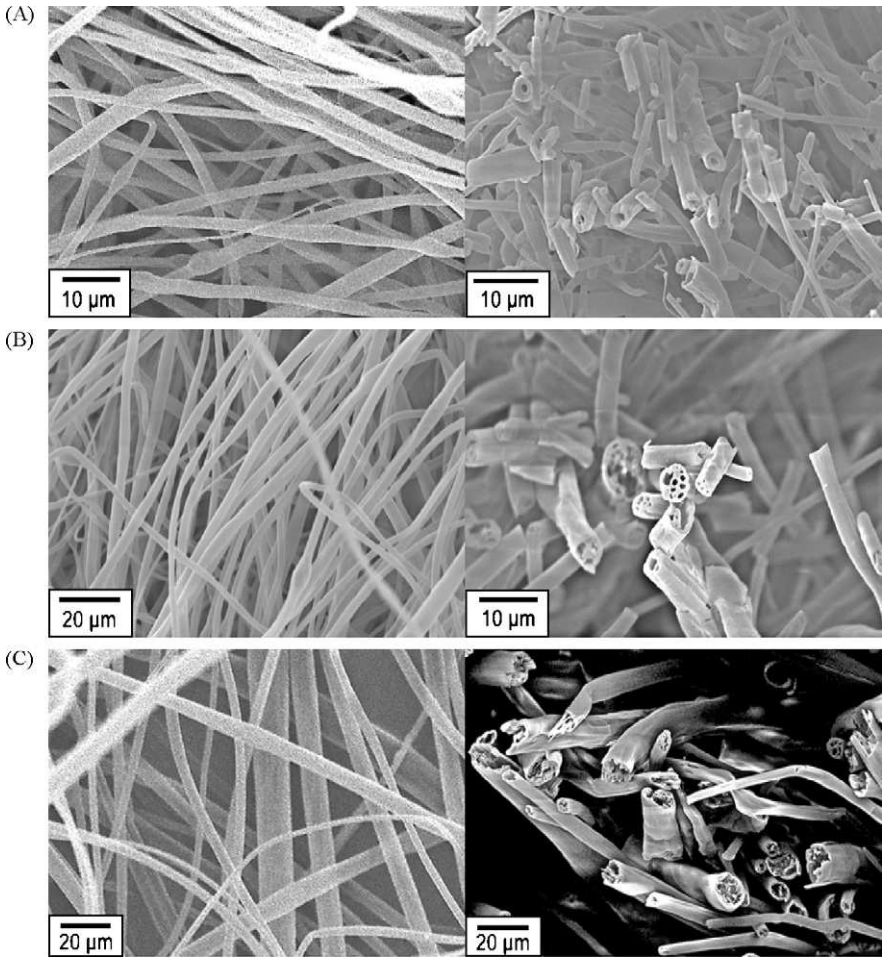

Fig. 4. SEM micrographs of PVP fibers (whole fibers in the left-side SEM and the same fibers cut open in the right-side SEM) created by electrospinning a 6.5 wt% PVP–DCM solution into CO_2 at room temperature (~22 °C) and 35 bar (A), 42 bar (B), and 50 bar (C).

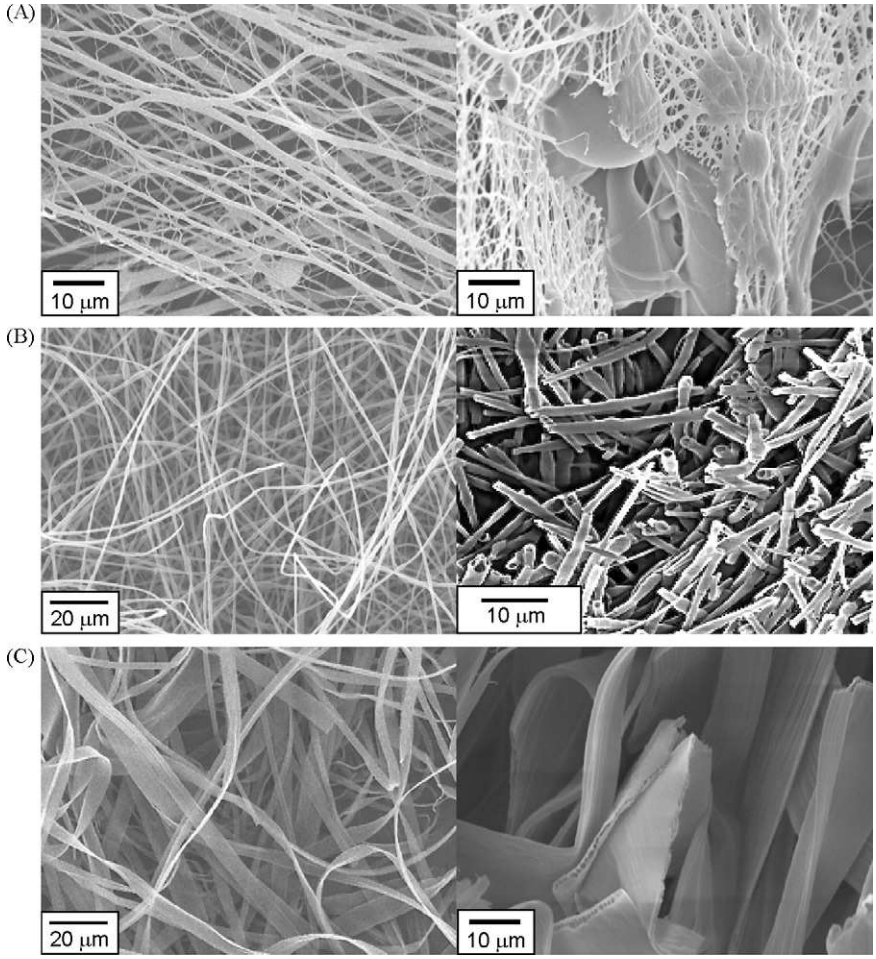

Fig. 5. SEM micrographs of PVP fibers created by electrospinning a 15 wt% PVP–ethanol solution into CO_2 at room temperature (~22 °C). (A) Two views of the fiber produced at 50 bar; (B) whole fibers in the left-side SEM and the same fibers cut open in the right-side SEM produced at 56 bar; (C) two views of the fiber produced at 65 bar with a close-up of the ribbons produced at this condition shown in the right-hand SEM.

further stretching the fibers to a smaller diameter as the jet travels from the nozzle to the target. These fibers have a smooth surface, a thin skin, and a very open-cell, porous interior. It is not possible to electrospin this solution at pressures greater than ~50 bar since the CO_2 extracts DCM so rapidly that the nozzle clogs. It is interesting that the threshold pressure for spinning into CO_2 is lower at the higher temperature of 34 °C. However, it is important to note that at the same operating pressure, the density of CO_2 is greater at 22 °C, the solubility of CO_2 into the PVP–DCM liquid jet is higher at the lower temperature, and since CO_2 behaves as a plasticizer that reduces the glass transition temperature of the polymer, the effect of CO_2 is greater at this slightly lower temperature. Hence, at the lower temperature of 22 °C, the liquid jet exhibits fluid-like properties even when operating at a slightly higher pressure. As the pressure is increased further at this lower temperature, the enhanced solvent power of CO_2 outweighs the plasticizing effect of pure CO_2 as significant amounts of DCM, a much better PVP plasticizer than CO_2, is extracted from the jet.

2.2. Electrospinning PVP–ethanol

Fig. 5 shows the PVP fibers created from electrospinning a 15 wt% PVP–ethanol solution at 22 °C. Since PVP readily dissolves in ethanol, the PVP–ethanol–CO_2 phase behavior is expected to be very similar to that shown in Fig. 2(D) for the PVP–DCM–CO_2 system. It is possible to electrospin this solution at ambient conditions in air and produce ~500 nm fibers although these fibers are not porous. However, it is not possible to create high-quality fiber with the apparatus shown in Fig. 1 if the CO_2 operating pressure is less than 42 bar. The polymer solution drips from the nozzle and even though some fibers are formed, these fibers are coated with large amounts of excess polymer. If the CO_2 operating pressure is increased to 50 bar, inter-connected fibers with a few beads are produced, as shown in Fig. 5(A). At a CO_2 operating pressure of 56 bar hollow core fibers are produced with diameters of ~1 μm (Fig. 5(B)). Some of these fibers have multiple pores although most have a single hollow core. If the solution is spun in saturated liquid CO_2 at ~65 bar, the fibers exhibit a ribbon-like morphology that are ~1 μm thick and ~20 μm wide. These ribbons also have numerous internal pores as shown in the right-hand SEM in Fig. 5(C). The mechanism for forming ribbons is not known at this time although this phenomenon has been seen in a few instances of electrospinning at ambient conditions.

Fibers, with diameters of ~300 nm and some beads, are produced by spinning a 5 wt% PVP–ethanol solution in air, as shown in Fig. 6(A). If the same solution is electrospun at a CO_2 operating pressure of 56 bar, slightly smaller diameter fibers are produced although again a significant amount of beads are also produced as shown in Fig. 6(B). When the solution is electrospun into saturated liquid CO_2 at a pressure of ~65 bar, porous fibers are produced as shown in Fig. 6(C) and (D). Some of these fibers are cylindrical while other fibers exhibit a more flattened, ribbon-like morphology. It is interesting that when electrospinning 15 and 5 wt% PVP–ethanol solutions the nozzle does not clog even though the solubility of

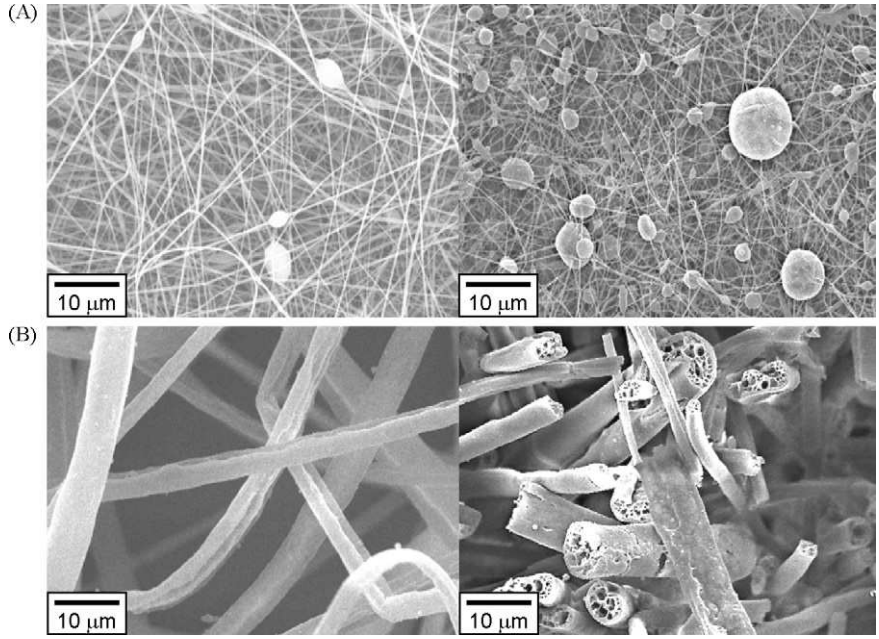

Fig. 6. SEM micrographs of PVP fibers created by electrospinning a 5 wt% PVP–ethanol solution into CO_2 at room temperature (~22 °C) and ambient (A), 56 bar (B), and 65 bar (C and D).

ethanol in CO_2 [47] is similar to that of DCM at the same temperature and pressure. Evidently the interaction of ethanol with PVP plays an important role in determining the "spinnability" of PVP in CO_2.

2.3. Electrospinning PVDF–DMAc and PVDF–DMF

As previously mentioned, it is problematic to electrospin difficult-to-dissolve polymers, such as poly(vinylidene fluoride) (PVDF), that dissolve in very low volatility solvents. However, it is possible to create porous PVDF fibers using the ES–PCA technique with CO_2. If a 20 wt% PVDF–DMAc solution is electrospun at ambient conditions in the open environment, the polymer jet is still wet (Fig. 7(A)) when it reaches the target due to the low volatility of DMAc and the relatively short nozzle-to-target distance. At a CO_2 pressure of 56 bar, dry fibers are produced as shown in Fig. 7(B). When the pressure of CO_2 was increased to the saturation pressure, ~65 bar, porous fibers are produced as shown in Fig. 7(C) and (D). The fiber diameters are in the range of 1–5 μm. Porous fibers are also formed when electrospinning a 15 wt% PVDF–DMAc solution into saturated CO_2 vapor as shown in Fig. 7(D).

Similar PVDF fiber morphologies are produced from 15 wt% PVDF–DMF solutions spun into CO_2 and the same trends in fiber quality and morphology are observed with DMF as with DMAc. At room temperature it is not possible to create dry fiber until the pressure gets close to the CO_2 saturation pressure. If the jet is spun

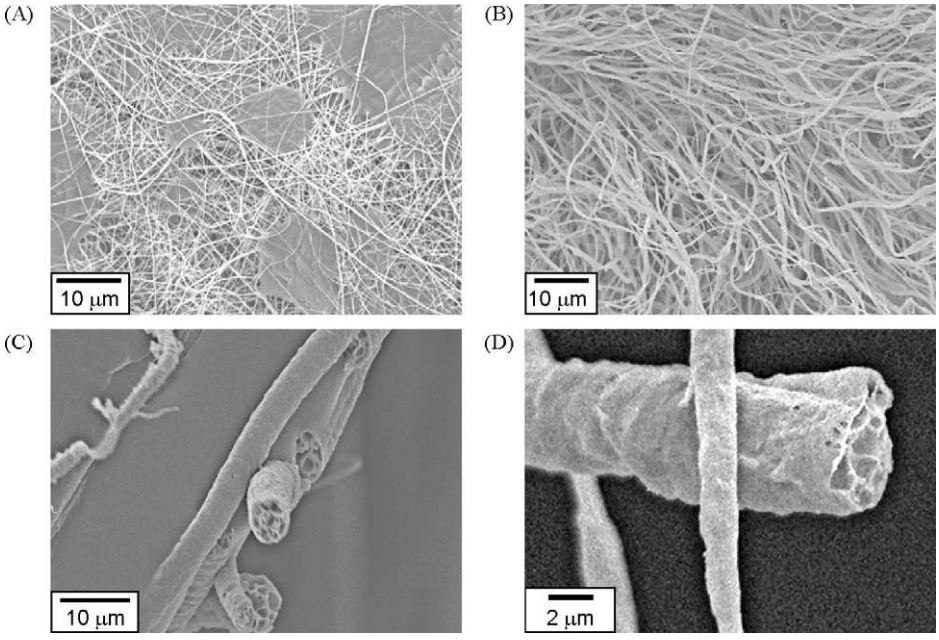

Fig. 7. SEM micrographs of PVDF fibers created by electrospinning a 20 wt% PVDF–DMAc solution into CO_2 at room temperature (~22 °C) and ambient pressure (A), 56 bar (B), and 65 bar (C). SEM micrograph of PVDF fibers created by electrospinning a 15 wt% PVDF–DMAc solution into CO_2 at room temperature (~22 °C) and 65 bar (D).

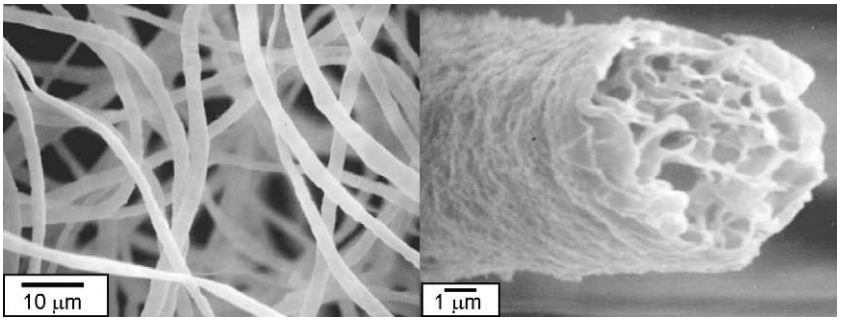

Fig. 8. SEM micrographs of PVDF fibers created by electrospinning a 15 wt% PVDF–DMF solution into CO_2 at 42 °C and 90 bar.

into saturated liquid CO_2, the nozzle clogs as the CO_2 dries the jet too quickly. At ~40 °C it is possible to create porous fiber at CO_2 pressures between 75 and 90 bar. At pressures near 75 bar the fiber diameter is smaller than that obtained at ~90 bar. However, porous PVDF fiber is obtained, as shown in Fig. 8, if the operating pressure is increased to ~90 bar. Notice also that the skin on the PVDF fibers in Fig. 7(C) and (D), and Fig. 8(B) are not nearly as smooth as those of the PVP fibers. PVDF has a melting point of ~165 °C while PVP is amorphous. As CO_2 extracts solvent away from the PVDF–solvent jet, PVDF can crystallize. As the fiber is being pulled toward the target the amorphous regions of the PVDF skin are being stretched and the crystalline regions of PVDF are sliding along the surface. If the solidification of PVDF can be suppressed while electrospinning, it should be possible to create smaller diameter fibers before the PVDF locks in a particular diameter.

2.4. Discussion

Hollow and open-cell fibers are created in the PCA process when the outer fiber skin is rapidly formed, the diffusion of the solvent is subsequently suppressed, and the sorption of CO_2 into the jet induces the solution trapped inside the fiber to phase separate allowing CO_2-rich voids to form and grow [26,27]. As previously mentioned, this mechanism is also applicable to the fibers formed in the present study for the ES–PCA process. Fig. 9 shows a schematic diagram of the proposed mechanism for the formation of porous and hollow fibers in the ES–PCA process used in the present study. CO_2 extracts the polymer solvent on the surface of the jet and a solid skin forms very rapidly (stage 1) similar to a wet-spinning process or asymmetric membrane preparation process where polymer solutions are coagulated in a nonsolvent [48–50]. As more CO_2 diffuses into the jet, the polymer solution trapped inside the jet phase separates into polymer-rich and polymer-lean phases initially by a nucleation and growth mechanism (see Fig. 9, stages 2 and 3), but very quickly the CO_2 concentration becomes high enough to induce spinodal decomposition of the solution. The polymer–solvent network in the interior of the jet, is still fluid-like since it contains a significant amount of liquid solvent that slowly diffuses through the skin. The fluid-like polymer–solvent solution offers little resistance to the growth of CO_2-rich voids that begin to coalesce as more CO_2 diffuses into the jet (Fig. 9, stage 4). The jet diameter is continually reduced as it travels to the target due to the action of electrodynamic forces. The stretching of the jet promotes the coalescence of the CO_2-rich bubbles which displace the polymer-rich network from the center of the jet ultimately resulting in the formation of a hollow fiber (Fig. 9, stages 5 and 6). The final internal morphology of the fiber depends on the time-of-flight of the jet traveling from the nozzle to the target, the initial concentration of the polymer solution, and the CO_2 pressure, which fixes the path followed in a polymer–solvent–antisolvent (CO_2) ternary phase diagram during spinodal decomposition [26,51].

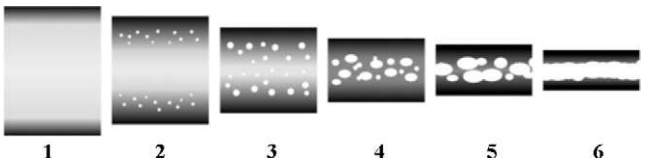

Fig. 9. Hollow and open-cell fiber formation mechanism for the electrospinning–PCA process used in the present study. The dark shading indicates a high, local concentration of polymer. 1, skin formation noted by the darker region; 2, nucleation of polymer-rich phase (darker region), solvent-rich phase (lighter regions), and CO_2-rich phase (white bubbles); 3, growth of CO_2-rich phase; 4, coalescence of CO_2-rich bubbles; 5, further coalescence of CO_2-rich bubbles – if the process stops here an open-cell structure is created; 6, hollow fiber formation.

Fibers with a hollow core are created if the "effective" glass transition temperature, T_g, of the polymer remains below the operating temperature which would allow the polymer network to be displaced from the inner surface of the fiber by the CO_2-rich bubbles. If the solvent power of CO_2 is too high, the polymer solvent is removed so rapidly from the jet that the polymer-rich network vitrifies and exhibits an increased modulus before the CO_2-rich bubbles can displace the polymer-rich phase from the center of the fiber. In this instance the polymer network freezes into the open-cell structure. As previously mentioned, at even higher CO_2 operating pressures the nozzle clogs due to the very rapid removal of polymer solvent from the liquid jet. Hence, elevated operating pressures are neither desired nor practical for this ES–PCA process. It is also worth noting that the hollow and open-cell fibers prepared by the combined ES–PCA technique have diameters at least one order of magnitude smaller than those prepared by the PCA technique alone. Also, the fiber diameter could likely be reduced further if the nozzle-to-target distance is increased.

2.5. Conclusions

In our previous study [22], the fibers created with the shorter nozzle-to-collector distance had a much different morphology than the fibers obtained with the new apparatus described here. The solid and porous fibers created with the original apparatus had diameters of ~20 μm, which is an order of magnitude larger than the fibers obtained in the present work. With the new apparatus, the polymer jet experiences longer flight times due to the longer nozzle-to-collector distance, which allows more time for the fibers to stretch and elongate before depositing on the collector. In contrast with the original apparatus, the electrospinning jet only evolve to stages 4 or 5 in Fig. 9 by the time the jet reaches the collector. Consequently, the fiber diameter was larger and the pores inside the fiber did not coalesce completely, which results in an open-cell morphology [22]. With the ES–PCA process it is possible to obtain different fiber morphologies by adjusting the pressure of CO_2 which affects the rate of solution phase separation during the flight time of the electrospinning jet. The ES–PCA technique has the advan-

tage that fiber morphology can be easily controlled via pressure and, as described here, extreme pressures are not needed to obtain a variety of different fiber morphologies. Since the ES–PCA operating pressures and temperatures are so mild, this new process offers the possibility to work with living cells in order to design Celloidosomes(r) fibers [52].

Acknowledgments

The SEM micrographs were done on instrumentation in the VCU Department of Neurobiology and Anatomy Microscopy Facility, supported, in part, with funding from the NIH-NINDS Center core grant (5P30NS047463). MM gratefully acknowledges partial funding for this work from the Fundacion Seneca-Agencia de Ciencia y Tecnologia as part of the II PCTRM 2007–2010 program.

References

[1] C. Burger, B.S. Hsiao, B. Chu, Nanofibrous materials and their applications, Annual Review of Materials Research 36 (2006) 333–368.
[2] Z.M. Huang, Y.Z. Zhang, M. Kotaki, S. Ramakrishna, A review on polymer nanofibers by electrospinning and their applications in nanocomposites, Composites Science and Technology 63 (2003) 2223–2253.
[3] D.H. Reneker, A.L. Yarin, E. Zussman, H. Xu, Electrospinning of nanofibers from polymer solutions and melts, Advances in Applied Mechanics 41 (2007) 43–195.
[4] S. Ramakrishna, K. Fujihara, W.-E. Teo, T.-C. Lim, Z. Ma, An Introduction to Electrospinning and Nanofibers, World Scientific Publishing, Singapore, 2005.
[5] D. Li, Y.N. Xia, Electrospinning of nanofibers: reinventing the wheel? Advanced Materials 16 (2004) 1151–1170.
[6] J. Doshi, D.H. Reneker, Electrospinning process and applications of electrospun fibers, Journal of Electrostatics 35 (1995) 151–160.
[7] T. Subbiah, G.S. Bhat, R.W. Tock, S. Pararneswaran, S.S. Ramkumar, Electrospinning of nanofibers, Journal of Applied Polymer Science 96 (2005) 557–569.
[8] S. Ramakrishna, K. Fujihara, W.E. Teo, T. Yong, Z.W. Ma, R. Ramaseshan, Electrospun nanofibers: solving global issues, Materials Today 9 (2006) 40–50.
[9] M. Bognitzki, H.Q. Hou, M. Ishaque, T. Frese, M. Hellwig, C. Schwarte, A. Schaper, J.H. Wendorff, A. Greiner, Polymer, metal, and hybrid nano- and mesotubes by coating degradable polymer template fibers (TUFT process), Advanced Materials 12 (2000) 637.
[10] M. Bognitzki, W. Czado, T. Frese, A. Schaper, M. Hellwig, M. Steinhart, A. Greiner, J.H. Wendorff, Nanostructured fibers via electrospinning, Advanced Materials 13 (2001) 70.
[11] S. Megelski, J.S. Stephens, D.B. Chase, J.F. Rabolt, Micro- and nanostructured surface morphology on electrospun polymer fibers, Macromolecules 35 (2002) 8456–8466.
[12] C.L. Casper, J.S. Stephens, N.G. Tassi, D.B. Chase, J.F. Rabolt, Controlling surface morphology of electrospun polystyrene fibers: effect of humidity and molecular weight in the electrospinning process, Macromolecules 37 (2004) 573–578.
[13] J.T. McCann, M. Marquez, Y.N. Xia, Highly porous fibers by electrospinning into a cryogenic liquid, Journal of American Chemical Society 128 (2006) 1436–1437.
[14] M. Bognitzki, T. Frese, M. Steinhart, A. Greiner, J.H. Wendorff, A. Schaper, M. Hellwig, Preparation of fibers with nanoscaled morphologies: electrospinning of polymer blends, Polymer Engineering and Science 41 (2001) 982–989.
[15] D. Li, Y.N. Xia, Direct fabrication of composite and ceramic hollow nanofibers by electrospinning, Nano Letters 4 (2004) 933–938.
[16] I.G. Loscertales, A. Barrero, M. Marquez, R. Spretz, R. Velarde-Ortiz, G. Larsen, Electrically forced coaxial nanojets for one-step hollow nanofiber design, Journal of American Chemical Society 126 (2004) 5376–5377.
[17] J.T. McCann, D. Li, Y.N. Xia, Electrospinning of nanofibers with core-sheath, hollow, or porous structures, Journal of Materials Chemistry 15 (2005) 735–738.
[18] S.H. Zhan, D.R. Chen, X.L. Jiao, C.H. Tao, Long TiO_2 hollow fibers with mesoporous walls: sol–gel combined electrospun fabrication and photocatalytic properties, Journal of Physical Chemistry B 110 (2006) 11199–11204.
[19] E. Zussman, A.L. Yarin, A.V. Bazilevsky, R. Avrahami, M. Feldman, Electrospun polyacrylonitrile/poly (methyl methacrylate)-derived turbostratic carbon micro-/nanotubes, Advanced Materials 18 (2006) 348.
[20] A.F. Ismail, L.P. Yean, Review on the development of defect-free and ultrathin-skinned asymmetric membranes for gas separation through manipulation of phase inversion and rheological factors, Journal of Applied Polymer Science 88 (2003) 442–451.
[21] P. van de Witte, P.J. Dijkstra, J.W.A. van den Berg, J. Feijen, Phase separation processes in polymer solutions in relation to membrane formation, Journal of Membrane Science 117 (1996) 1–31.
[22] Z.H. Shen, B.E. Thompson, M.A. McHugh, Electrospinning in near-critical CO_2, Macromolecules 39 (2006) 8553–8555.
[23] M.A. McHugh, V.J. Krukonis, Supercritical Fluid Extraction: Principles and Practice, 2nd ed., Butterworth-Heinemann, Stoneham, 1994.
[24] C.F. Kirby, M.A. McHugh, Phase behavior of polymers in supercritical fluid solvents, Chemical Reviews 99 (1999) 565–602.
[25] W. Bae, S. Kwon, H.S. Byun, H. Kim, Phase behavior of the poly(vinyl pyrrolidone) + n-vinyl-2-pyrrolidone + carbon dioxide system, Journal of Supercritical Fluids 30 (2004) 127–137.
[26] D.J. Dixon, K.P. Johnston, Formation of microporous polymer fibers and oriented fibrils by precipitation with a compressed fluid antisolvent, Journal of Applied Polymer Science 50 (1993) 1929–1942.
[27] G. Luna-Barcenas, S.K. Kanakia, I.C. Sanchez, K.P. Johnston, Semicrystalline microfibrils and hollow fibers by precipitation with a compressed-fluid antisolvent, Polymer 36 (1995) 3173–3182.
[28] A.R. Berens, G.S. Huvard, R.W. Korsmeyer, F.W. Kunig, Application of compressed carbon dioxide in the incorporation of additives into polymers, Journal of Applied Polymer Science 46 (1992) 231–242.
[29] C. Anolick, E.P. Goffinet, Separation of ethylene copolymer elastomers from their solvent solutions, US Patent 3,553,156 (1971).
[30] P.I. Freeman, J.S. Rowlinson, Lower critical points in polymer solutions, Polymer 1 (1960) 20–26.
[31] C.A. Irani, C. Cosewith, S. Kasegrande, New method for high temperature phase separation of solutions containing copolymer elastomers, US Patent 4,319,021 (1982).
[32] M.A. McHugh, T.L. Guckes, Separating polymer solutions with supercritical fluids, Macromolecules 18 (1985) 680–687.
[33] M.J. Lazzaroni, D. Bush, J.S. Brown, C.A. Eckert, High-pressure vapor-liquid equilibria of some carbon dioxide + organic binary systems, Journal of Chemical and Engineering Data 50 (2005) 60–65.
[34] I. Tsivintzelis, D. Missopolinou, K. Kalogiannis, C. Panayiotou, Phase compositions and saturated densities for the binary systems of carbon dioxide with ethanol and dichloromethane, Fluid Phase Equilibria 224 (2004) 89–96.
[35] D.Y. Peng, D.B. Robinson, A new two-constant equation of state, Industrial Engineering Chemistry Research Fundamentals 15 (1976) 59–64.
[36] S.W. Choi, J.R. Kim, Y.R. Ahn, S.M. Jo, E.J. Cairns, Characterization of electrospun PVdF fiber-based polymer electrolytes, Chemistry of Materials 19 (2007) 104–115.
[37] H.J. Chung, D.W. Lee, S.M. Jo, D.Y. Kim, W.S. Lee, Electrospun poly(vinylidene fluoride)-based carbon nanofibers for hydrogen storage, Material Research Symposium Proceedings 837 (2005), N3.15.11–N13.15.16.
[38] J.R. Kim, S.W. Choi, S.M. Jo, D.W. Lee, B.C. Kim, Electrospun PVdF-based fibrous polymer electrolytes for lithium ion polymer batteries, Electrochimica Acta 50 (2004) 69–75.
[39] W.A. Yee, M. Kotaki, Y. Liu, X. Lu, Morphology, polymorphism behavior and molecular orientation of electrospun poly(vinylidene fluoride) fibers, Polymer 48 (2007) 512–521.
[40] Z. Zhao, J. Li, X. Yuan, X. Li, Y. Zhang, J. Sheng, Preparation and properties of electrospun poly(vinylidene fluoride) membranes, Journal of Applied Polymer Science 97 (2005) 466–474.
[41] H.S. Byun, N.-S. Jeon, Phase behavior measurement of the binary carbon dioxide-n-n-dimethylacetamide and carbon dioxide-n,n-diethylacetamide systems at high pressures, Fluid Phase Equilibria 167 (2000) 113–122.
[42] A. Kordikowski, A.P. Schenk, R.M. van Nielen, C.J. Peters, Volume expansions and vapor–liquid equilibria of binary mixtures of a variety of polar solvent and certain near-critical solvents, Journal of Supercritical Fluids 8 (1995) 205–216.
[43] R.W. Nichols, Pressure Vessel Codes and Standards, Elsevier, London, 1987.
[44] M.A. LoStracco, S.-H. Lee, M.A. McHugh, Comparison of the effect of density and hydrogen bonding on the cloud-point behavior of poly(ethylene-co-methyl acrylate)-propane–cosolvent mixtures, Polymer 35 (1994) 3272–3277.
[45] M.G. McKee, G.L. Wilkes, R.H. Colby, T.E. Long, Correlations of solution rheology with electrospun fiber formation of linear and branched polyesters, Macromolecules 37 (2004) 1760–1767.
[46] H. Fong, I. Chun, D.H. Reneker, Beaded nanofibers formed during electrospinning, Polymer 40 (1999) 4585–4592.
[47] M. Stievano, N. Elvassore, High-pressure density and vapor–liquid equilibrium for the binary systems carbon dioxide–ethanol, carbon dioxide–acetone and carbon dioxide–dichloromethane, Journal of Supercritical Fluids 33 (2005) 7–14.
[48] H.-S. Kim, K.-Y. Kim, H.-J. Jin, I.-J. Chin, Electrospinning using liquid reservoir collector, polymer preprints, American Chemical Society Division of Polymer Chemistry 45 (2004) 843–844.
[49] I. Pinnau, B.D. Freeman, Formation and modification of polymeric membranes: overview, ACS Symposium Series 744 (2000) 1–22.
[50] E. Smit, U. Buttner, R.D. Sanderson, Continuous yarns from electrospun fibers, Polymer 46 (2005) 2419–2423.
[51] J.O. Werling, P.G. Debenedetti, Numerical modelling of mass transfer in the supercritical antisolvent process, Journal of Supercritical Fluids 16 (1999) 167–181.
[52] M. Marquez, S. Marquez, A. Garcia, Celloidosomes, Viroidosomes, vesciodosomes, lipoidosomes, and method for their manufacture, US Provisional Patent 61/165,989. b) M. Marquez, S. Marquez, A. Garcia, Artificial microglandsÜS Provisional Patent 61/275,666. c) Celloidosomes (r) US Patent and Trade Office, Registry Number 3,738,109.